Transmission Performance of Chirp-Controlled Signal by Using Semiconductor Optical Amplifier

Toshio Watanabe, *Member, IEEE*, Norio Sakaida, Hiroshi Yasaka, *Member, IEEE*, Fumiyoshi Kano, *Member, IEEE*, and Masafumi Koga, *Member, IEEE*

***Abstract*—We examine the fiber transmission performance of the optical signal whose chirp is controlled by utilizing phase modulation in semiconductor optical amplifier (SOA) with both simulations and experiments. This chirp control technique converts a positive chirp created by electroabsorption (EA) modulator into negative chirp, which reduces the waveform degradation due to the chromatic dispersion in transmission over standard single-mode fiber (SMF). It also provides an optical gain that is sufficient to compensate the insertion loss of the EA modulator. We investigate how the chirp control is affected by the input power to the SOA and the carrier lifetime of the SOA. As the SOA input power increases, the negative chirp becomes large, while the waveform is largely distorted due to gain saturation. However, the waveform distortion at high SOA input powers can be shaped by using a frequency discriminator. The acceleration of the carrier lifetime also reduces the waveform distortion due to gain saturation. We demonstrate that the chirp control technique is effective even for a high bit rate optical signal up to 10 Gb/s, when the carrier lifetime is expedited by optical pumping.**

***Index Terms*—Chirp, electroabsorption (EA) modulators, optical fibers, phase modulation, semiconductor optical amplifiers (SOA's).**

I. Introduction

ELECTROABSORPTION (EA) modulator [1], [2] is attracting much attention as the external optical intensity modulator to be used in optical communication systems. This is because it has advantages of small size, low drive voltage and polarization insensitivity, compared with $LiNbO_3$ electrooptic modulator. The ease of integration with a laser enables us to realize a compact optical transmitter [3]–[6]. EA modulator is also suitable for use in opto-electronic wavelength conversion in the photonic transport system (PTS) node [7], where a received (incoming) optical signal is translated into a light selected out of those from a multiwavelength laser array by an optical switch. In this scheme, the modulater must be polarization insensitive.

A chirp of the modulator is a critical issue when a high bit-rate optical signal is transmitted through standard single-mode fiber (SMF). Positive chirp degrades the optical waveform in conjunction with the anomalous chromatic dispersion, and limits the signal transmission distance. The EA modulator exhibits chirp parameter that depends on bias voltage and wavelength [8]. Deep prebias and small detuning from the exciton peak offer a negative chirp operation of the EA modulator [9], [10], while both cause an increase in insertion loss. When a semiconductor optical amplifier (SOA) is placed after the EA modulator, we can convert the positive chirp into negative chirp [11] utilizing phase modulation in SOA [12]. This technique enables us to control the chirp created by the EA modulator, and also provides an optical gain that compensates the insertion loss of the EA modulator and other optical devices. Furthermore, the SOA can be integrated with the EA modulator. Its compactness is advantageous for use in the PTS node, where the loss is compensated for each optical path (for example, 8 wavelengths $\times$ 16 ports $=$ 128 paths), if necessary.

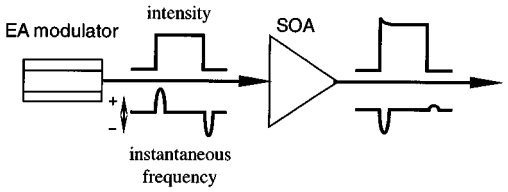

Fig. 1. Schematics of chirp control using SOA.

In this paper, we examine this chirp control technique with both simulations and experiments. Section II describes the simulation of chirp control using SOA. We exhibit that phase modulation in SOA converts the positive chirp created by an EA modulator into negative chirp, and it improves the signal transmission distance in SMF. The dependence on the input power to the SOA and the carrier lifetime of the SOA is also investigated. Section III presents the experimental results which verify the effect of the chirp control. Section IV describes the impact of the loss compensation in PTS nodes by using SOA. The final section is conclusions.

II. Simulation of Chirp Control

In this section, we describe the simulation of chirp control using SOA. Fig. 1 shows the schematics of the chirp control. The optical signal launched into an EA modulator is injected into an SOA in order to control the chirp.

A. Chirp Parameter of SOA

First, we describe the chirp parameter of SOA. The chirp parameter α [13] is defined as

$$\alpha = 2I \frac{d\Phi}{dI} \tag{1}$$

Manuscript received December 14, 1999; revised May 11, 2000.

T. Watanabe was with NTT Network Innovation Laboratories, Kanagawa 239-0847, Japan. He is now with NTT Photonics Laboratories, Ibaraki 319-1193, Japan.

N. Sakaida was with NTT Network Innovation Laboratories, Kanagawa 239-0847, Japan. He is now with NTT Communications Corporation, Japan.

H. Yasaka was with NTT Network Innovation Laboratories, Kanagawa 239-0847, Japan. He is now with NTT Electronics Corporation, Japan.

F. Kano, and M. Koga are with NTT Network Innovation Laboratories, Kanagawa 239-0847, Japan.

Publisher Item Identifier S 0733-8724(00)06479-3.

where I and Φ are optical intensity and phase of output electric field, respectively. In SOA, both intensity change ΔI and phase change $\Delta\Phi$ are caused by carrier density change ΔN. The carrier density N is determined by the rate equation

$$\frac{dN}{dt} = -\frac{N}{\tau} - A_g(N - N_0)\frac{I}{h\nu} + \frac{J}{ed} \tag{2}$$

and optical intensity I is determined by

$$\frac{dI}{dz} = \Gamma A_g(N - N_0) \tag{3}$$

where τ, A_g, N_0, $h\nu$, J, e, d, and Γ are carrier lifetime, differential gain, transparent carrier density, photon energy, injection current density, electron charge, active layer thickness, and optical confinement factor, respectively.

Assuming that ΔN is uniform in SOA, gain change ΔG (in dB units) and $\Delta\Phi$ are expressed as

$$\Delta G = 10\log_{10} e \cdot \Gamma A_g \Delta N L, \tag{4}$$

and

$$\Delta\Phi = -\frac{2\pi}{\lambda}\Delta n L = \frac{\alpha'}{2}\Gamma A_g \Delta N L \tag{5}$$

where λ, n and L are wavelength, refractive index and device length, respectively. And α' is the linewidth enhancement factor of semiconductor material, which is defined as

$$\alpha' = -\frac{4\pi}{\lambda}\frac{(\partial n/\partial N)}{\Gamma A_g}. \tag{6}$$

From (1), (4) and (5), we can obtain the chirp parameter of the SOA as

$$\alpha = \alpha'\frac{dG}{dP_{\text{out}}} = \alpha'\frac{(dG/dP_{\text{in}})}{1 + (dG/dP_{\text{in}})} \tag{7}$$

where P_{in} and P_{out} are the SOA input and output power, respectively. When the optical input power is low enough, (7) gives $\alpha = 0$ because the carrier density remains unchanged to the value at the equilibrium ($\Delta N = 0$) and $dG/dP_{\text{in}} = 0$. However, as the optical input power increases, carrier depletion occurs in SOA ($\Delta N < 0$) and this induces gain saturation ($dG/dP_{\text{in}} < 0$). Since $\alpha' > 0$ in gain medium such as SOA, the chirp parameter is negative ($\alpha < 0$) for the SOA under gain-saturated condition.

B. Dynamic Chirp Control

We calculated the optical output waveform and instantaneous optical frequency change of SOA by solving (2) and (3) numerically. In this calculation, we divided the SOA into ten sections in order to take the nonuniform distribution of carrier density into consideration. The bit rate of optical signal is 2.5 Gb/s, and the electrical bandwidths of both the electrical signal and EA modulator are 10 GHz. Here the carrier lifetime of SOA is 200 ps (the dependence on the carrier recovery time is discussed in Section II-E). Fig. 2(a) shows the optical intensity waveform before and after SOA. The SOA input powers are set at $P_s - 6$ dB, $P_s - 3$ dB, and P_s, where P_s is the 3 dB gain saturation input power. Fig. 2(b) shows the instantaneous optical frequency change when the optical signal without any chirp ($\alpha = 0$) is introduced to the SOA. After the SOA, the instantaneous frequency falls at the leading edge of the optical signal and rises at the trailing edge. This is because the chirp parameter of the SOA is negative, as expected from (7). As the SOA input power increased, the optical frequency shifts more largely toward a lower frequency side. Fig. 2(c) shows the instantaneous frequency change before and after SOA when the optical signal launched from an EA modulator is introduced into SOA. Here the chirp parameter of the EA modulator varies from $+1.6$ at mark level to 0 at space level, corresponding to an effective chirp parameter [8] of $\alpha_{\text{eff}} = +1$. Before SOA, its instantaneous optical frequency rises at the leading edge and falls at the trailing edge, that is, the optical signal has a positive chirp. After passing through the SOA, the instantaneous optical frequency falls at the leading edge. This indicates that the positive chirp is converted into the negative chirp using SOA.

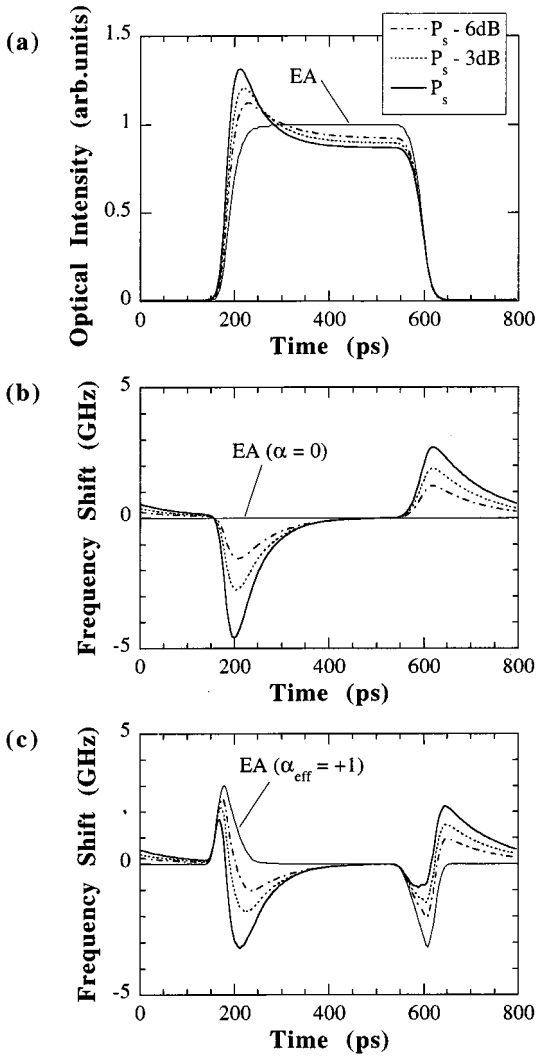

Fig. 2. (a) Calculated optical intensity waveform and instantaneous optical frequency change when (b) $\alpha = 0$ and (c) $\alpha_{\text{eff}} = +1$. Thin solid line: EA modulator output. Dotted–dashed line: after SOA ($P_{\text{in}} = P_s - 6$ dB). Dotted line: after SOA ($P_{\text{in}} = P_s - 3$ dB). Thick solid line: after SOA ($P_{\text{in}} = P_s$).

C. Eye Opening Penalty after Fiber Transmission

We calculated the transmission performance of the 2.5-Gb/s nonreturn-to-zero (NRZ) optical signal over standard SMF,

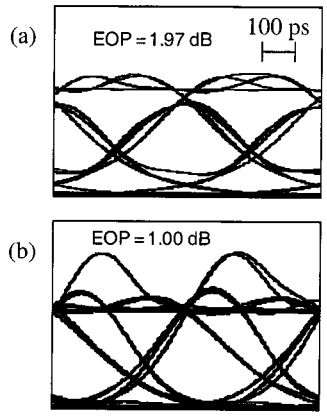

Fig. 3. Calculated eye pattern after 1000-km SMF transmission for (a) optical signal with positive chirp ($\alpha_{\rm eff} = +1$) and (b) chirp-controlled signal by SOA ($P_{\rm in} = P_s$).

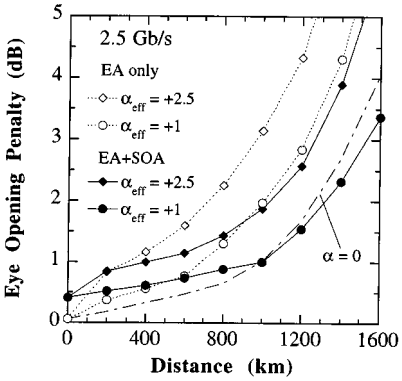

Fig. 4. Eye opening penalty as a function of SMF transmission distance. Dot-dashed line: chirpless signal ($\alpha = 0$). Dotted lines: optical signal with positive chirp (open diamonds: $\alpha_{\rm eff} = +2.5$; open circles: $\alpha_{\rm eff} = +1$). Solid lines: chirp-controlled signal by SOA (solid diamonds: $\alpha_{\rm eff} = +2.5$; solid circles: $\alpha_{\rm eff} = +1$).

whose chromatic dispersion is +17 ps/nm/km. Fig. 3 shows the calculated eye pattern after 1000-km SMF transmission. As shown in Fig. 3(a), the optical signal with a positive chirp ($\alpha_{\rm eff} = +1$) induces waveform broadening in conjunction with anomalous chromatic dispersion, resulting in a degraded eye pattern. In this case, the eye opening penalty (EOP) is 1.97 dB. Fig. 3(b) shows the eye pattern of the optical signal whose chirp is controlled to be negative by SOA. Here the SOA input power is P_s. The chirp-controlled signal exhibits better eye opening after SMF transmission, and EOP reduces to 1.00 dB.

Fig. 4 shows the EOP as a function of SMF transmission distance. The optical signal with positive chirp ($\alpha_{\rm eff} = +1$) exhibits a larger penalty than the signal without any chirp ($\alpha = 0$). To the contrary, when chirp is controlled by SOA, a penalty increase with transmission distance is smaller than the chirpless signal, although the gain saturation in SOA causes a slight (~0.4 dB) eye closure before SMF transmission. Then the signal transmission performance over dispersive optical fiber is improved by using the chirp control technique.

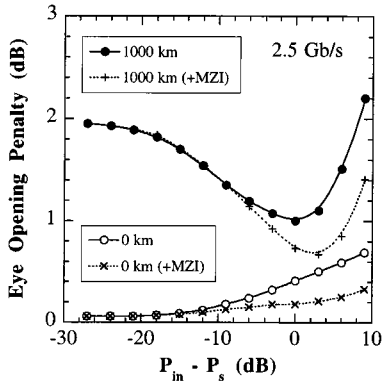

Fig. 5. Eye opening penalty as a function of SOA input power. Open circles: before transmission. Solid circles: after 1000 km SMF transmission. Crosses (×): before transmission with waveform shaping by MZI. Crosses (+): after 1000 km SMF transmission with waveform shaping by MZI.

D. Dependence on SOA Input Power

As shown in Fig. 2, the change in optical frequency depends on the input power to the SOA. Fig. 5 shows EOP before and after 1000-km SMF transmission as a function of the SOA input power. Before transmission, EOP becomes larger as the input power increases because of the waveform distortion due to the gain saturation. After SMF transmission, a minimum EOP is obtained when the SOA input power is around P_s. When the SOA input power is so low that the waveform distortion is negligible, the EOP after SMF transmission decreased as the input power increases, because the negative frequency shift increases and this reduces the dispersion penalty. However, the SOA input power exceeds P_s, the SOA output waveform is strongly distorted due to the gain saturation, resulting in an increase in EOP after SMF transmission. It is noted that P_s generally depends on a bias current of the SOA and operating wavelength [14]. As the bias current is increased, P_s increases as well as the optical gain. To minimize the wavelength dependence, we should set the SOA gain peak on the shorter side of operating wavelength.

The EOP increase at high SOA input powers can be reduced by shaping the distorted waveform using Mach–Zehnder interferometer (MZI) as a frequency discriminator [15]. Fig. 6(a) shows the schematics of the waveform shaping using MZI. As shown in Fig. 6(b), the transmission peak of the MZI is set at somewhat higher than the optical signal frequency, so that the transmission of the MZI decreases as the optical frequency decreases. When the distorted optical signal is introduced to the MZI before SMF transmission, the signal suffers some attenuation at the leading edge, since the optical frequency shifts toward a lower frequency side. We calculated the optical intensity waveform before and after the MZI. A 2.5-Gb/s optical signal is at first introduced to the SOA at an input power of P_s, and then passed through the MZI whose free spectral range (FSR) is 50, 100, and 200 GHz, respectively. The detuning of the MZI is set at 1/4 of FSR. As shown in Fig. 7, the waveform distortion at the leading edge is shaped by using the MZI. This reduces the EOP before and after SMF transmission even at high SOA input powers, as shown in Fig. 5.

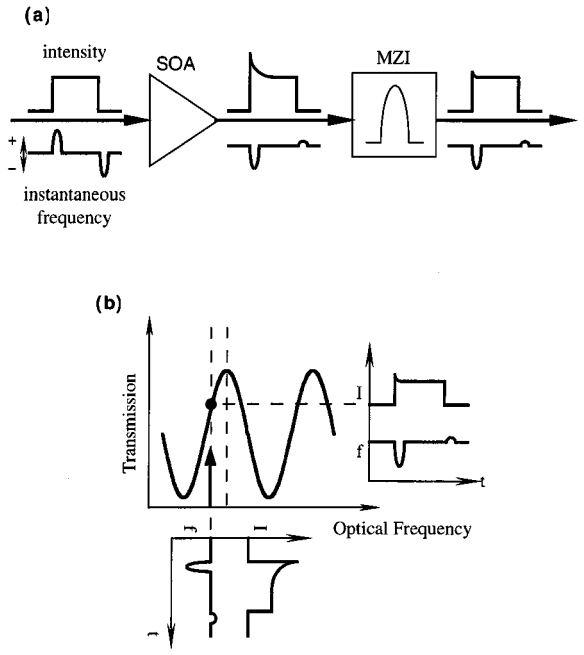

Fig. 6. (a) Schematics of the waveform shaping using MZI. (b) Frequency setting of MZI.

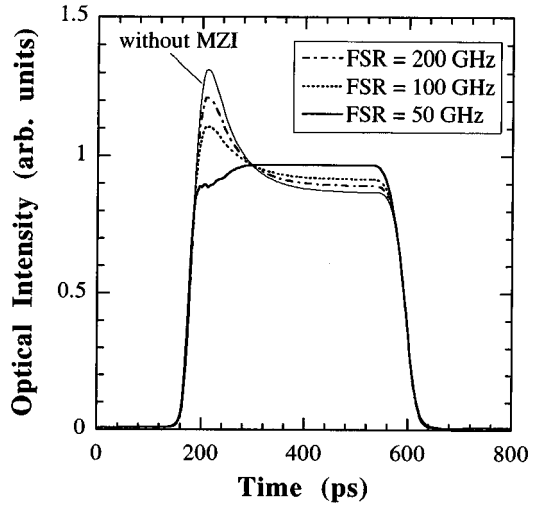

Fig. 7. Calculated optical intensity waveform after MZI's with different FSR. Thin solid line: without MZI. Dotted-dashed line: MZI output (FSR $=$ 200 GHz). Dotted line: MZI output (FSR $=$ 100 GHz). Thick solid line: after SOA MZI output (FSR $=$ 50 GHz).

E. Dependence on Carrier Lifetime of SOA

The waveform distortion due to gain saturation in SOA can be also reduced by accelerating the carrier lifetime τ_s of SOA. Although a typical value of τ_s is 200 ps, we can make it shorter by means of optical pumping [16] or carrier injection (i.e., high bias current) [14]. Fig. 8 shows the intensity waveform and frequency shift of 2.5-Gb/s optical signal as a parameter of τ_s. Here the SOA input power is set at P_s. As τ_s is decreased, the waveform distortion at the leading edge is reduced. The frequency

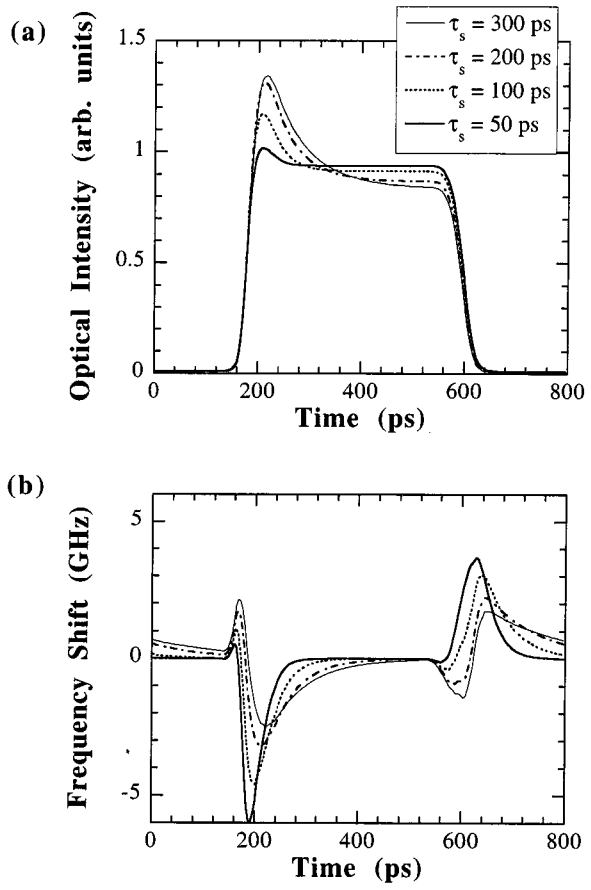

Fig. 8. (a) Calculated optical intensity waveform and (b) instantaneous optical frequency as a parameter of carrier lifetime τ_s.

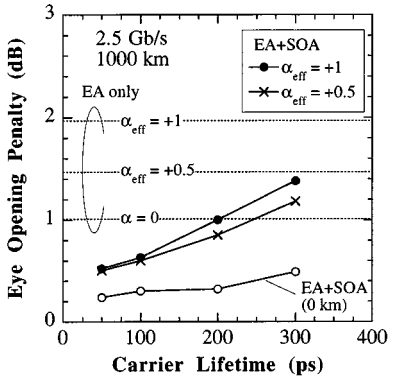

Fig. 9. Eye opening penalty as a function of carrier lifetime. Dotted lines: after 1000-km SMF transmission without SOA. Open circles: before transmission with SOA. Solid lines: after 1000-km SMF transmission with SOA (solid circle: $\alpha_{\rm eff} = +1$, crosses: $\alpha_{\rm eff} = +0.5$).

shifts rapidly, and the amount of the peak frequency shift increases. Fig. 9 shows the EOP before and after 1000-km SMF transmission as a function of τ_s. A decrease in τ_s results in the decrease in EOP both before and after transmission. When τ_s is less than 200 ps and 250 ps (1/2 and 5/8 of the time slot of a 2.5-Gb/s NRZ signal), the same EOP (1.0 dB) as $\alpha = 0$ is obtained for $\alpha_{\rm eff} = +1$ and $+0.5$, respectively.

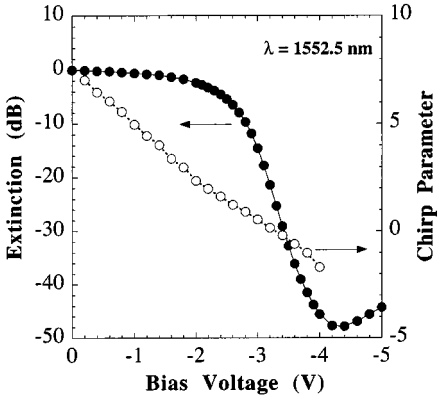

Fig. 10. Optical extinction (solid circles) and chirp parameter (open circles) of the EA modulator used here as a function of the bias voltage.

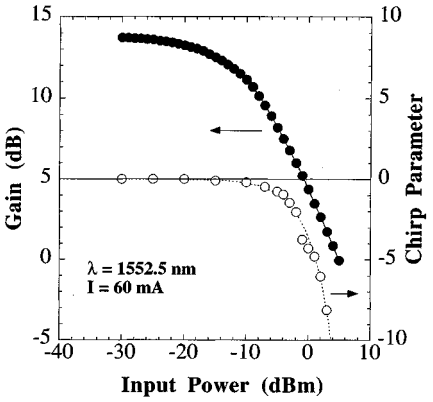

Fig. 11. Measured chirp parameter (open circles) and optical gain (solid circles) of the SOA used here as a function of the optical input power.

III. Experiment

A. Chirp Parameter of EA Modulator and SOA

We measured the chirp parameter using the fiber response peak method described in [17]. Fig. 10 shows the optical extinction and chirp parameter of the EA external modulator used here as a function of the bias voltage. The polarization sensitivity of the EA modulator was <1 dB. The photoluminescence peak was 1.47 μm, which was detuned $\sim$80 nm from the 1.55-μm wavelength band. When the reverse bias voltage was changed from -0.8 V to -3.8 V, its chirp parameter varied from $+5.6$ to -1.0, resulting an effective chirp parameter [8] of $+3.1$.

The SOA used here had an optical gain band whose peak wavelength was 1540 nm and 3-dB bandwidth was $\sim$60 nm at a bias current of 60 mA. Fig. 11 shows the measured chirp parameter and optical gain of the SOA as a function of the optical input power at a wavelength of 1552.5 nm. The unsaturated optical gain was 13 dB, and it was insensitive to polarization ($<$0.5 dB) owing to a bulk active layer with square cross section. The 3-dB saturation input power was -9 dBm. When the input power became larger than this value, the chirp parameter of the SOA rapidly fell to a negative value, and exceeded -5 at an input power of $+2$ dBm. This negative chirp of SOA was utilized to control the chirp of the optical signal of the EA modulator.

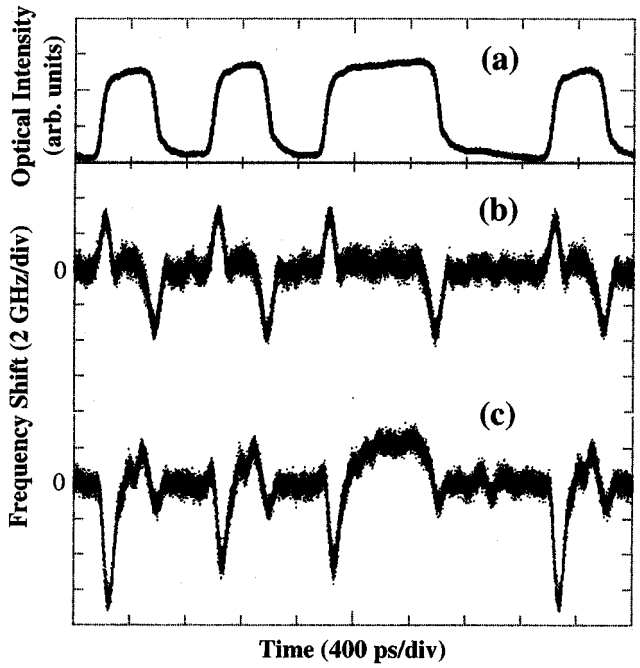

Fig. 12. (a) Measured intensity waveform launched from the EA modulator. Measured instantaneous optical frequency change (b) before introducing SOA and (c) after passing through SOA.

B. Dynamic Chirp Measurement

We measured an instantaneous optical frequency change using an optical frequency discriminator composed of a PLC-type MZI with dual p-i-n photodetectors. A fixed NRZ pulse pattern of 2.5 Gb/s was applied to the EA modulator. A bias voltage and a swing voltage were -2.3 and 3.0 V_{p-p}, respectively. The insertion loss of the EA modulator was 8 dB under this drive condition, excluding a 3-dB intrinsic encoding loss. Fig. 12(a) shows the optical intensity waveform launched from the EA modulator. The instantaneous frequency raised at the leading edge of the optical signal and fell at the falling edge, as shown in Fig. 12(b), indicating that the optical signal had positive chirp. Then the optical signal with positive chirp was injected into the SOA at the average input power of -7 dBm. After passing through the SOA, the instantaneous frequency fell at the leading edge, as shown in Fig. 12(c). This indicates that the positive chirp of the optical signal was successfully converted into negative chirp using the chirp control technique, as expected by the simulation.

C. Optical Fiber Transmission

We verified the effect of the chirp control in transmission of a 2.5-Gb/s NRZ [pseudorandom binary sequence (PRBS) $2^{23}-1$] signal across SMF whose chromatic dispersion was $+17$ ps/nm/km. Fig. 13 shows the schematics of the transmission experiment. The optical signal power injected to the booster Er-doped fiber amplifier (EDFA) was set at -25 dBm both with and without the chirp control. We employed inline EDFA's spaced at 100 km intervals, and the span loss was set at 28 dB for each 100 km SMF. The fiber input power from both the booster and inline EDFA's was set at $+3$ dBm. In order to

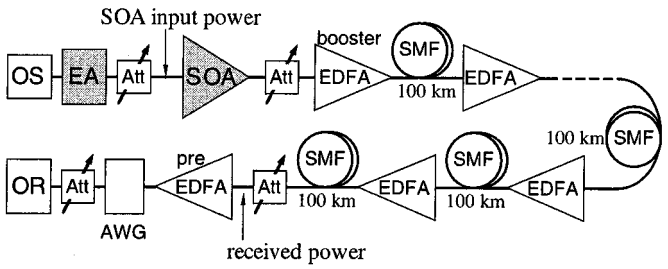

Fig. 13. Schematics of transmission experiment.

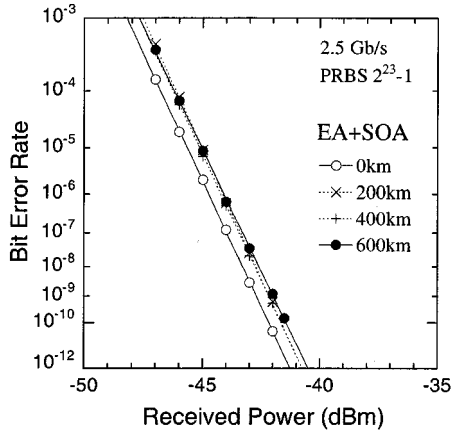

Fig. 14. BER of 2.5-Gb/s signal as a function of received optical power.

remove ASE from the EDFA's, we placed a planar lightwave circuit (PLC)-type arrayed waveguide grating filter in front of the optical receiver. The threshold voltage of the receiver was fixed throughout this experiment.

Fig. 14 shows the bit error rate (BER) of the chirp-controlled signal as a function of the received optical power. The average input power of the SOA was set at −12 dBm, that is, the optical input power at mark level was −9 dBm (P_s). In this condition, the SOA provides an optical gain of 10 dB, which was sufficient to compensate the insertion loss of the EA modulator. The optical signal exhibited no error floor even after signal transmission over 600-km SMF, and the power penalty at a BER of 10^{-9} was less than 1 dB. This result shows that the chirp control technique using the SOA is effective for extending the signal transport distance in SMF. Fig. 15 shows the measured transmission penalty as a function of distance. The optical signal without chirp control exhibited larger penalty than that with chirp control. This result qualitatively matched the simulation described in Section II-C.

We measured the dependence on input power to the SOA. Fig. 16 shows the penalty before and after 400-km SMF transmission as a function of the average SOA input power. Both before and after transmission, the minimum penalty was obtained at an average input power of −12 dBm. The penalty increase at low SOA input powers were attributed to the signal-to-noise ratio (SNR) degradation due to amplified spontaneous emission (ASE). An increase in the input power above −12 dBm caused the increase in the penalty due to the waveform distortion, as expected by the simulation. In order to shape the distortion, we used a PLC-type MZI as a frequency discriminator [15]. The

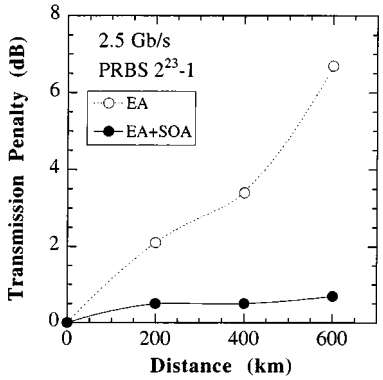

Fig. 15. Measured transmission penalty as a function of distance. Open circles: EA modulator without chirp control. Solid circles: with chirp control by SOA.

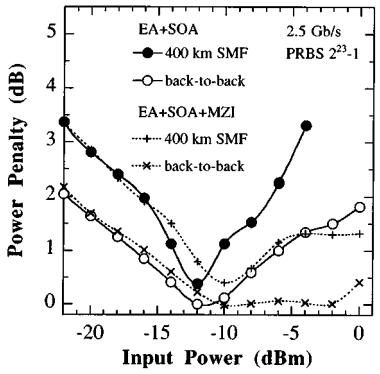

Fig. 16. Measured penalty of the chirp-controlled signal as a function of SOA input power. Open circles: back-to-back measurement. Solid circles: after 400-km SMF transmission. Crosses (×): back-to-back measurement with waveform shaping by MZI. Crosses (+): after 400-km SMF transmission with waveform shaping by MZI.

MZI had a free spectral range of 50 GHz, and its transmission peak of the MZI was set at 8 GHz higher than the optical signal frequency. When the distorted waveform was shaped by using the MZI, the penalty before SMF transmission remained around zero over input powers up to −2 dBm, as shown in Fig. 16. The waveform shaping by MZI reduced the penalty after transmission at high SOA input powers, as expected by the simulation. This technique was effective without changing the SOA bias current even when operating wavelength was switched at 200-GHz spaced eight channels ranged from 1546 to 1557 nm [15].

D. Transmission of 10 Gb/s Optical Signal

In Section II-E, we have shown by simulation that the chirp control using SOA was effective when the carrier lifetime τ_s was less than ∼200 ps for a 2.5-Gb/s signal. If we apply the chirp control technique to a 10-Gb/s optical signal, τ_s (typically 200 ps) must be expedited to be ∼50 ps. In this experiment, we made τ_s shorter by means of optical injection to the SOA [16]. When a cw light of +5 dBm was injected to the SOA, τ_s was estimated to be 70 ps. Here we used the EA modulator whose effective chirp parameter [8] was +0.4. The output power of the booster EDFA was set at +8 dBm, and no in-line amplifier was used. The threshold voltage of the receiver was optimized

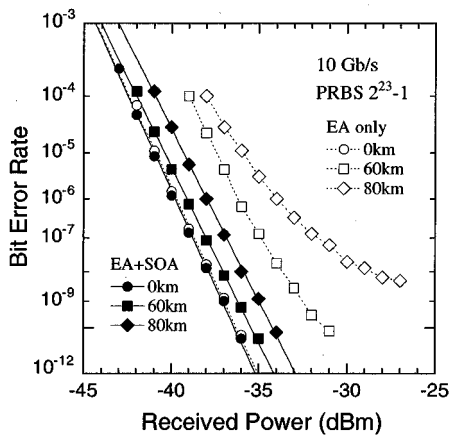

Fig. 17. BER of 10-Gb/s signal as a function of received optical power.

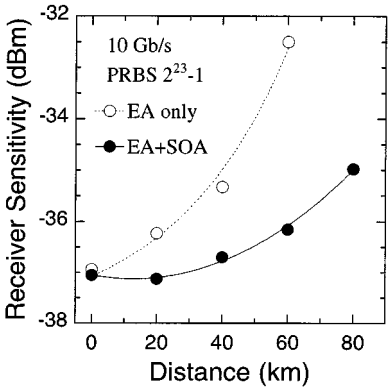

Fig. 18. Receiver sensitivity of 10-Gb/s signal as a function of distance. Solid circles: EA modulator without chirp control. Open circles: with chirp control by SOA.

for each back-to-back measurement with and without chirp control. Fig. 17 shows the BER of 10-Gb/s NRZ (PRBS $2^{23}-1$) signal with and without chirp control. Without chirp control, the transmission distance in SMF was limited to within 40 km, and error floor was observed over 60 km. To the contrary, the optical signal with chirp control can be transmitted over 80 km SMF. Fig. 18 shows the receiver sensitivity as a function of transmission distance. The results indicate that the chirp control using SOA is also effective for 10 Gb/s signal when τ_s is expedited.

IV. Loss Compensation in PTS Node

When the SOA is employed in the rear of the EA modulator in a PTS node, it not only controls the chirp of the optical signal, as described in previous chapter, but also enhances the signal power level. Here we will discuss the impact of loss compensation in a PTS node by using SOA's. Fig. 19(a) shows the block diagram of the PTS node we considered. The WDM signals launched to the PTS node through the incoming optical fiber are amplified by a pre-OA, demultiplexed into individual optical channel and then received by an OR. The received signal is regenerated electrically and fed into an EA modulator. The EA modulator inscribed the signal in a continuous-wave (CW)

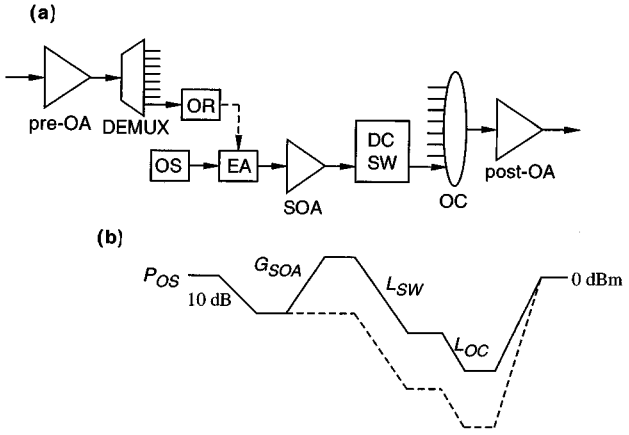

Fig. 19. (a) Block diagram of PTS node. (b) Level diagram of PTS node.

light from an optical source (OS). The OS is a distributed feedback laser diode (DFB-LD) for the PTS node without wavelength conversion, while that is a tunable DBR-LD for the PTS node with wavelength conversion. A multiwavelength DFB-LD array with a wavelength selective switch (WS–SW) [7] can be used instead of the tunable LD. The optical signal launched from the EA modulator is amplified by an SOA, and routed by an $N \times M$ delivery-and-coupling type optical switch (DC–SW). The DC–SW comprises of $1 \times N$ optical switches and $1 \times M$ optical couplers (OC). Here M is the number of WDM channels, and N is the number of incoming/outgoing fibers. Then the signals are combined by an $N \times 1$ OC, amplified by a post-OA, and then sent into an outgoing fiber.

We calculated the SNR at the output of PTS node (i.e., the output of post-OA) and after 320 km (80 km $\times$ 4 span) fiber transmission. The level diagram is shown in Fig. 19(b). The OS output power is $P_{\rm OS}$ and the loss of the EA modulator is 10 dB. The SOA has a noise figure (NF) of 10 dB. The insertion losses of the DC–SW and OC are $L_{\rm SW}$ and $L_{\rm OC}$, respectively. The NF's of both post- and inline OA are 7 dB, and that of the pre-OA is 5 dB. The fiber input power is 0 dBm, and the span loss is 28 dB. Fig. 20 shows the calculated Q-factor as a function of SOA gain. The calculation is done for $P_{\rm OS} = 0$ dBm, -5 dBm and -10 dBm, which correspond to the SOA input power of -10 dBm, -15 dBm and -20 dBm, respectively. Here we set $L_{\rm SW} + L_{\rm OC} = 30$ dB, because the reported loss value for an 8×16 PTS node is $L_{\rm SW} = 14$ dB and $L_{\rm OC} = 13$ dB [18], and we took into account the margin of 3 dB. The Q-factor increases as the SOA gain increases. When the SOA is not used, the Q-factor after 320 km transmission becomes less than 17 dB (corresponding to the BER of 10^{-12}) for $P_{\rm OS} = 0$ dBm. This is because the optical power at the input of the post-OA is as low as -40 dBm and the Q-factor at the node output is 18 dB. To the contrary, when the SOA is employed, the Q-factor after 320 km transmission becomes higher than 17 dB. When $P_{\rm OS}$ is decreased to -5 and -10 dBm, the SOA is required to have a gain of larger than 5 dB and 10 dB, respectively, in order to obtain $Q^2 > 17$ dB.

The required gain value can be tolerated when the EA modulator and the SOA are integrated together. Assuming that the coupling loss between an EA modulator (or SOA) chip and an

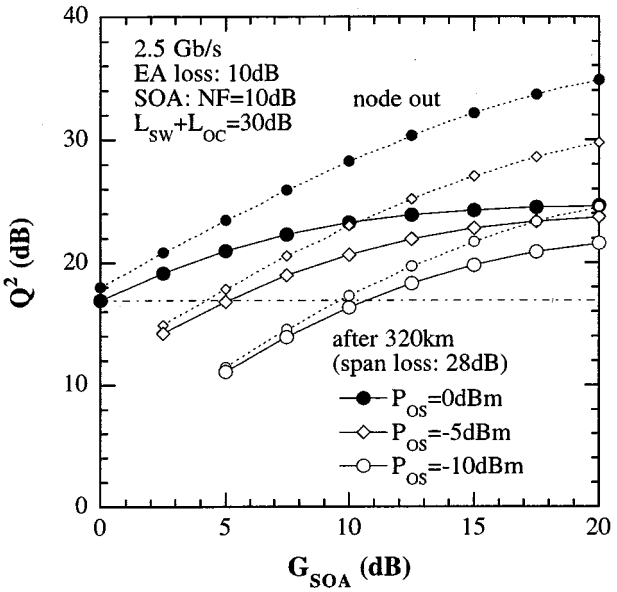

Fig. 20. Q-factor as a function of SOA gain for $P_{\rm OS} = 0$ dBm (solid circles), $P_{\rm OS} = -5$ dBm (open triangles), and $P_{OS} = -10$ dBm (open circles). Dotted line: at the node output. Solid line: after 320-km fiber transmission.

optical fiber is 3 dB/facet and the coupling loss between the EA modulator and SOA is 1 dB, the required (internal) gain of SOA is reduced by 5 dB.

V. Conclusion

We examined the fiber transmission performance of the optical signal whose chirp was controlled by using SOA with both simulations and experiments. A positive chirp created by EA modulator was successfully converted into negative chirp, which was advantageous for SMF transmission. The SOA input power and the carrier lifetime affected the chirp control. As the SOA input power increases, the negative chirp became large, while the waveform was largely distorted due to gain saturation. However, the waveform distortion at high SOA input powers can be shaped by using a frequency discriminator. The acceleration of the carrier lifetime also reduces the waveform distortion due to gain saturation. We demonstrate that the chirp control technique is effective even for a 10-Gb/s optical signal, when the carrier lifetime is expedited by optical pumping.

This chirp control technique using SOA also provided an optical gain that compensated the insertion loss of the passive optical components used in PTS node. We believe that this technique will enhance the performance of photonic transport networks effectively.

Acknowledgment

The authors would like to thank N. Takachio, T. Kawai, K.-I Sato, and H. Yoshimura for their fruitful discussions.

References

[1] T. Ido, S. Tanaka, M. Suzuki, M. Koizumi, H. Sano, and H. Inoue, "Strained InGaAs/InAlAs MQW electro-absorption optical modulators with large bandwidth and low driving voltage," *IEEE Photon. Technol. Lett.*, vol. 6, pp. 1207–1209, Oct. 1994.

[2] K. Wakita, I. Kotaka, K. Yoshino, S. Kondo, and Y. Noguchi, "Polarization-independent electroabsorption modulators using strain-compensated InGaAs–InAlAs MQW structures," *IEEE Photon. Technol. Lett.*, vol. 7, pp. 1418–1420, Dec. 1995.

[3] K. Morito, R. Sahara, K. Sato, and Y. Kotaki, "Penalty-free 10 Gb/s NRZ transmission over 100 km of standard fiber at 1.55 μm with a blue-chirp modulator integrated DFB laser," *IEEE Photon. Technol. Lett.*, vol. 8, pp. 431–433, Mar. 1996.

[4] Y. K. Park, T. V. Nguyen, P. A. Morton, J. E. Johnson, O. Mizuhara, J. Jeong, L. D. Tzeng, P. D. Yeates, T. Fullowan, P. F. Sciortino, A. M. Sergent, W. T. Tsang, and R. D. Yadvish, "Dispersion-penalty-free transmission over 130-km standard fiber using a 1.55-μm, 10-Gb/s integrated EA/DFB laser with low-extinction ratio and negative chirp," *IEEE Photon. Technol. Lett.*, vol. 8, pp. 1255–1257, Sept. 1996.

[5] H. Takeuchi, K. Tsuzuki, K. Sato, M. Yamamoto, Y. Itaya, A. Sano, M. Yoneyama, and T. Otsiji, "NRZ operation at 40Gb/s of a compact module cantaining an MQW electroabsorption modulator integrated with a DFB laser," *IEEE Photon. Technol. Lett.*, vol. 9, pp. 572–574, May 1997.

[6] M. Ishizaka, M. Yamaguchi, J. Shimizu, and K. Komatsu, "The transmission capability of a 10-Gb/s electroabsorption modulator integrated DFB laser using the offset bias chirp reduction technique," *IEEE Photon. Technol. Lett.*, vol. 9, pp. 1628–1630, Dec. 1997.

[7] T. Kawai, M. Teshima, H. Yasaka, M. Kobayashi, and M. Koga, "Wavelength selectable photonic transport system applicable to unequal channel spacing," in *Proc. ECOC'98*, Paper WdD26.

[8] F. Dorgeuille and F. Devaux, "On the transmission performances and the chirp parameter of a multiple-quantum-well electroabsorption modulator," *IEEE Quantum Electron.*, vol. 30, pp. 2565–2572, Nov. 1994.

[9] J. A. J. Fells, M. A. Gibbon, I. H. White, G. H. B. Thompson, R. V. Penty, C. J. Armistead, E. A. Kimber, D. J. Moule, and E. J. Thrush, "Transmission beyond the dispersion limit using a negative chirp electroabsorption modulator," *Electron. Lett.*, vol. 30, no. 14, pp. 1168–1169, 1994.

[10] K. Yamada, K. Nakamura, Y. Matsui, T. Kunii, and Y. Ogawa, "Negative-chirp electroabsorption modulator using low-wavelength detuning," *IEEE Photon. Technol. Lett.*, vol. 7, pp. 1157–1158, Oct. 1995.

[11] T. Watanabe, N. Sakaida, H. Yasaka, and M. Koga, "Chirp control of optical signal using phase modulation in semiconductor optical amplifier," *IEEE Photon. Technol. Lett.*, vol. 10, pp. 1027–1029, July 1998.

[12] G. P. Agrawal and N. A. Olsson, "Amplification and compression of weak picosecond optical pulses by using semiconductor-laser amplifier," *Opt. Lett.*, vol. 14, no. 10, pp. 500–502, 1989.

[13] F. Koyama and K. Iga, "Frequency chirping in external modulators," *J. Lightwave Technol.*, vol. 6, pp. 87–92, Jan. 1988.

[14] K. Inoue, "Semiconductor laser amplifiers," in *Optical Amplifiers and Their Applications*, S. Shimada and H. Ishio, Eds. New York: Wiley, 1994, ch. 3.

[15] T. Watanabe, H. Yasaka, N. Sakaida, and M. Koga, "Waveform shaping of chirp-controlled signal by semiconductor optical amplifier using Mach-Zehnder frequency discriminator," *IEEE Photon. Technol. Lett.*, vol. 10, pp. 1422–1424, Oct. 1998.

[16] M. J. Manning, D. A. O. Davies, D. Cotter, and J. K. Lucek, "Enhanced recovery rates in semiconductor laser amplifiers using optical pumping," *Electron. Lett.*, vol. 30, no. 10, pp. 787–788, 1994.

[17] F. Devaux, Y. Sorel, and J. F. Kerdiles, "Simple measurement of fiber dispersion and chirp parameter of intensity modulated light emitter," *J. Lightwave Technol.*, vol. 11, pp. 1937–1940, Dec. 1993.

[18] M. Koga, A. Watanabe, T. Kawai, K.-I. Sato, and Y. Ohmori, "Large-capacity optical path cross-connect system for WDM photonic transport network," *IEEE J. Select. Areas Commun.*, vol. 16, July 1998.

Toshio Watanabe (M'98) received the B.E. and M.E. degrees in organic and polymeric materials engineering from Tokyo Institute of Technology, Japan, in 1990 and 1992, respectively.

In 1992, he joined the NTT Opto-electronics Laboratories, Tokai-mura, Japan, and worked on the development of polymeric materials for optical waveguide devices. From 1997 to 1999, he was at NTT Optical Network Systems Laboratories (now NTT Network Innovation Laboratories), Yokosuka, Japan, where he engaged in research on photonic network systems. He is now with the NTT Photonics Laboratories, Tokai-mura, Japan.

Mr. Watanabe is a member of the Japan Society of Applied Physics and the Institute of Electronics, Information and Communication Engineers (IEICE) of Japan.

Norio Sakaida was born in Aichi, Japan. He received the B.E. and M.E. degrees in applied physics from Tohoku University, Sendai, Japan, in 1992 and 1994, respectively.

In 1994, he joined the NTT Optical Network System Laboratories, NTT Corporation, Yokosuka-shi, Japan. During 1994-1998, he was engaged in research on photonic network technologies. Since 1999, he has developed video transmission system based on ATM techniques in Media Technology Development Center, NTT Communications Corporation.

Mr. Sakaida is a member of the Institute of Electronics, Information and Communication Engineers (IEICE) of Japan.

Hiroshi Yasaka (M'92) was born in Oita, Japan, in 1959. He received the B.S. and M.S. degrees in physics from Kyushu University, Fukuoka, Japan, in 1983 and 1985, and the Ph.D. degree in electronics engineering from Hokkaido University, Hokkaido, Japan, in 1993, respectively.

In 1985, he joined the Atsugi Electrical Communications Laboratories, Nippon Telegraph and Telephone (NTT) Corporation, Kanagawa, Japan. Since then, he has been engaging in research and development on semiconductor photonic devices mfor optical fiber communication systems. He is now with NTT Electronics Corporation.

Dr. Yasaka is a member of the Japan Society of Applied Physics and the Physical Society of Japan.

Fumiyoshi Kano (M'91) was born in Shizuoka, Japan, in 1963. He received the B.E., M.E., and Ph.D. degrees in applied physics from Tohoku University, Sendai, Japan, in 1985, 1987, and 1996, respectively.

In 1987, he joined NTT Electrical Communication Laboratories. Since then, he has been engaged in development research work on semiconductor lasers and their applications for photonic network systems.

Dr. Kano is a member of the Japan Society of Applied Physics and the Institute of Electronics, Information and Communication Engineers (IEICE) of Japan.

Masafumi Koga (M'89) was born in Fukuoka, Japan, on February 14, 1959. He received the B.E. and M.E. degrees in electronics engineering from the Kyushu Institute of Technology, Fukuoka, in 1981 and 1983, respectively, and received the Dr. Eng. degree from Osaka University, Osaka, in 1993.

In 1983, he joined the NTT Electrical Communications Laboratories, Yokosuka-shi, Japan, where from 1986 to 1992, he has developed the high-performance optical circulator and its functional circuits. Since 1994, he has been designing and developing a hardware system for realizing the photonic transport network.

Dr. Koga is a member of the Institute of Electronics, Information and Communication Engineers of Japan (IEICE).